BJP British Journal of Pharmacology

DOI:10.1111/bph.12215
www.brjpharmacol.org

RESEARCH PAPER

Role of the $K_{Ca}3.1$ K^+ channel in auricular lymph node $CD4^+$ T-lymphocyte function of the delayed-type hypersensitivity model

Susumu Ohya[1,2], Erina Nakamura[1], Sayuri Horiba[1], Hiroaki Kito[1], Miki Matsui[1], Hisao Yamamura[1] and Yuji Imaizumi[1]

[1]*Department of Molecular & Cellular Pharmacology, Graduate School of Pharmaceutical Sciences, Nagoya City University, Nagoya, Japan, and* [2]*Department of Pharmacology, Division of Pathological Sciences, Kyoto Pharmaceutical University, Kyoto, Japan*

Correspondence
Yuji Imaizumi, Molecular & Cellular Pharmacology, Graduate School of Pharmaceutical Sciences, Nagoya City University, 3-1 Tanabedori, Mizuhoku, Nagoya 467-8603, Japan. E-mail: yimaizum@phar.nagoya-cu.ac.jp

Keywords
intermediate-conductance Ca^{2+}-activated K^+ channel; $CD4^+$ T-lymphocyte; TRAM-34; delayed-type hypersensitivity; repressor element-1 silencing transcription factor; auricular lymph node

Received
11 May 2012
Revised
18 February 2013
Accepted
1 March 2013

BACKGROUND AND PURPOSE

The intermediate-conductance Ca^{2+}-activated K^+ channel ($K_{Ca}3.1$) modulates the Ca^{2+} response through the control of the membrane potential in the immune system. We investigated the role of $K_{Ca}3.1$ on the pathogenesis of delayed-type hypersensitivity (DTH) in auricular lymph node (ALN) $CD4^+$ T-lymphocytes of oxazolone (Ox)-induced DTH model mice.

EXPERIMENTAL APPROACH

The expression patterns of $K_{Ca}3.1$ and its possible transcriptional regulators were compared among ALN T-lymphocytes of three groups [non-sensitized (Ox–/–), Ox-sensitized, but non-challenged (Ox+/–) and Ox-sensitized and -challenged (Ox+/+)] using real-time polymerase chain reaction, Western blotting and flow cytometry. $K_{Ca}3.1$ activity was measured by whole-cell patch clamp and the voltage-sensitive dye imaging. The effects of $K_{Ca}3.1$ blockade were examined by the administration of selective $K_{Ca}3.1$ blockers.

KEY RESULTS

Significant up-regulation of $K_{Ca}3.1a$ was observed in $CD4^+$ T-lymphocytes of Ox+/– and Ox+/+, without any evident changes in the expression of the dominant-negative form, $K_{Ca}3.1b$. Negatively correlated with this, the repressor element-1 silencing transcription factor (REST) was significantly down-regulated. Pharmacological blockade of $K_{Ca}3.1$ resulted in an accumulation of the $CD4^+$ T-lymphocytes of Ox+/+ at the G_0/G_1 phase of the cell cycle, and also significantly recovered not only the pathogenesis of DTH, but also the changes in the $K_{Ca}3.1$ expression and activity in the $CD4^+$ T-lymphocytes of Ox+/– and Ox+/+.

CONCLUSIONS AND IMPLICATIONS

The up-regulation of $K_{Ca}3.1a$ in conjunction with the down-regulation of REST may be involved in $CD4^+$ T-lymphocyte proliferation in the ALNs of DTH model mice; and $K_{Ca}3.1$ may be an important target for therapeutic intervention in allergy diseases such as DTH.

Abbreviations

ALN, auricular lymph node; AP-1, activator protein-1; $DiBAC_4(3)$, bis-(1,3-dibutylbarbituric acid)trimethine oxonol; DTH, delayed-type hypersensitivity; FCM, flow cytometry; ICA-17043, 2,2-bis(4-fluorophenyl)-2-phenyl-acetamide; $K_{Ca}3.1$, intermediate-conductance Ca^{2+}-activated K^+ channel; REST, repressor element-1 silencing transcription factor; TRAM-34, 1-[(2-chlorophenyl)diphenylmethyl]-1H-pyrazole

Introduction

Ca^{2+}-activated K^+ channels play important roles in the cell proliferation and migration of various types of cells (Köhler *et al.*, 2003; Cruse *et al.*, 2006; Yamazaki *et al.*, 2006; Shepherd *et al.*, 2007; Chantome *et al.*, 2009). The intermediate-conductance Ca^{2+}-activated K^+ channel ($K_{Ca}3.1$) contributes to the driving force for the Ca^{2+} influx so as to trigger the T-cell activation (Chandy *et al.*, 2004; Cahalan and Chandy, 2009). The modification of $K_{Ca}3.1$ activity determines the Ca^{2+} response through the control of the membrane potential in T-lymphocytes (Ghanshani *et al.*, 2000; Chandy *et al.*, 2004; Nicolaou *et al.*, 2007). $K_{Ca}3.1$ is required for the activation of T helper 1 (Th1) and Th2 $CD4^+$ T-lymphocytes (Di *et al.*, 2010a,b), and is therefore a potential therapeutic target for disorders of the immune system (Jensen *et al.*, 2001; Chandy *et al.*, 2004; Cahalan and Chandy, 2009). We have recently identified an N-terminus-lacking $K_{Ca}3.1$ splice variant ($K_{Ca}3.1b$) from mammalian lymphoid tissues, which inhibits membrane trafficking of the full-length $K_{Ca}3.1a$ proteins via a dominant-negative effect on channel activity by interaction with $K_{Ca}3.1a$ to form heteromeric channels (Ohya *et al.*, 2011b). Transcriptional and post-translational modifications of $K_{Ca}3.1$ exert an effect on its channel activity in T-lymphocytes. In terms of transcriptional factors for $K_{Ca}3.1$, activator protein-1 (AP-1) (Fos/Jun heterodimers) and repressor element-1 silencing transcription factor (REST) have been identified (Ghanshani *et al.*, 2000; Cheong *et al.*, 2005). In activated T-lymphocytes, AP-1 causes an up-regulation of $K_{Ca}3.1$ by binding to the $K_{Ca}3.1$ promoter (Ghanshani *et al.*, 2000). A reduction in REST expression results in an up-regulation of $K_{Ca}3.1$ in undifferentiated smooth muscle cells (SMCs) (Cheong *et al.*, 2005). REST is ubiquitously expressed in various tissues (Gopalakrishnan, 2009), but it remains unclear whether REST functions as a potential regulator of $K_{Ca}3.1$ in the immune system. In terms of the post-translational modification of $K_{Ca}3.1$, several reports by Srivastava *et al.* (2005; 2006; 2008; 2009) have demonstrated potential negative and positive regulators of $K_{Ca}3.1$ in T-lymphocytes.

The pathophysiological significance of $K_{Ca}3.1$ in the immune system has been studied using pharmacological blockade and gene knockdown of $K_{Ca}3.1$. $K_{Ca}3.1$ blockers are potentially useful as treatment of sickle anaemia (Jensen *et al.*, 2001; Chandy *et al.*, 2004) and inflammatory bowel diseases (Di *et al.*, 2010a) and also as immunosuppressants (Jensen *et al.*, 2001; Chandy *et al.*, 2004; Pegoraro *et al.*, 2009). Loss of $K_{Ca}3.1$ causes the impairment of both Ca^{2+} influx and cytokine production in T-lymphocytes (Di *et al.*, 2010a), as well as progressive splenomegaly (Grgic *et al.*, 2009a). Tharp *et al.* (2006; 2008) have shown that up-regulation of the $K_{Ca}3.1$ gene followed by $K_{Ca}3.1$ promoter activation is involved in vascular SMC dedifferentiation; and pharmacological blockade of $K_{Ca}3.1$ induces the silencing of the $K_{Ca}3.1$ gene mediated through REST and AP-1.

Pegoraro *et al.* (2009) have shown that the $K_{Ca}3.1$ blocker, clotrimazole, inhibits ear swelling in an oxazolone (Ox)-induced delayed-type hypersensitivity (DTH) model, an animal model for contact allergy in the skin developed by Evans *et al.* (1971). Additionally, Di *et al.* (2010a) have shown that Ca^{2+} influx via Ca^{2+} release activating Ca^{2+} (CRAC) channels as a result of $K_{Ca}3.1$ activation is essential for IL-2 production in T-lymphocytes, and that $K_{Ca}3.1$ activity is markedly up-regulated following differentiation into Th1 cells. In the present study, we focused on the potential role of $K_{Ca}3.1$ and its transcriptional regulator(s) in $CD4^+$ T-lymphocytes isolated from the auricle lymph nodes (ALNs) of Ox-induced DTH model mice, and also on the effects of pharmacological $K_{Ca}3.1$ blockade of $K_{Ca}3.1$ and its transcriptional expression.

Methods

Preparation of Ox-induced DTH model mice

BALB/cCrSlc male mice, 5–6 weeks of age, were obtained from the breeding colony at Japan SLC (Hamamatsu, Shizuoka, Japan). All experiments were carried out in accordance with the guiding principles for the care and use of laboratory animals in Nagoya City University and Kyoto Pharmaceutical University, and also with the approval of the Presidents of both universities. The mice were skin-sensitized 7 days after the last day of irradiation by a topical application to the shaved abdomen of 100 μL of 0.5% Ox in acetone. Control mice were sham-sensitized by a topical application of 100 μL of acetone. Seven days after sensitization, the right ear was challenged with a topical application of 10 μL of 0.5% Ox in acetone. Mice received s.c. injections of TRAM-34 (1-[(2-chlorophenyl)diphenylmethyl]-1H-pyrazole; 3 or 10 $mg \cdot kg^{-1}$, s.c.) or vehicle (dimethylsulfoxide) at the time of challenge. Ear thickness was measured prior to and 24 h after the challenge with an engineer's micrometer. Auricular lymph nodes (ALNs) were dissected and were then used for expression and/or functional analyses. For expression analysis, tissues were stored at –80°C until use.

RNA extraction, reverse transcription-polymerase chain reaction (PCR) and real-time PCR

Total RNA extraction and reverse transcription-PCR (RT-PCR) were performed as previously reported (Ohya *et al.*, 2005). The resulting cDNA product was amplified with gene-specific primers; and the primers are designed using Primer Express™ software (Ver 1.5, Applied Biosystems, Foster City, CA, USA). Quantitative, real-time PCR was performed with the use of Syber Green chemistry (SYBR® *Premix Ex Taq*™ II; Takara, Osaka, Japan) on an ABI 7700 sequence detector system (Applied Biosystems) as previously reported (Ohya *et al.*, 2011b). PCR primers used are shown in the Supporting Information. Regression analyses of the mean values of three multiplex RT-PCRs for the $\log_{10}$ diluted cDNA were used to generate standard curves. Unknown quantities relative to the standard curve for a particular set of primers were calculated, yielding transcriptional quantitation of the gene products relative to the endogenous standard, β-actin. To confirm the nucleotide sequences, the amplified PCR products and plasmid constructs were sequenced with an ABI PRIZM 3100 genetic analyser (Applied Biosystems).

Measurement of membrane potential by the voltage-sensitive dye imaging

Mice were sacrificed and the ALNs were isolated and processed individually. Single-cell suspensions were prepared by pressing

the lymph node with frosted glass slides. The membrane potential was measured using the voltage-sensitive dye, bis-(1,3-dibutylbarbituric acid)trimethine oxonol [$DiBAC_4(3)$], as previously reported (Funabashi *et al.*, 2010). Prior to the fluorescence measurements with $DiBAC_4(3)$, the isolated cells were incubated in normal HEPES buffer containing 100 nM $DiBAC_4(3)$ for 20 min at room temperature. The stained cells were continuously incubated with 100 nM $DiBAC_4(3)$ throughout the experiments. Data collection and analysis were performed using an ARUGUS-HiSCA imaging system (Hamamatsu Photonics, Hamamatsu, Shizuoka, Japan).

Electrophysiological recordings

The whole-cell patch clamps was applied to single $CD4^+$ T-lymphocytes using CEZ-2400 amplifier (Nihon Kohden, Tokyo, Japan) at room temperature (23 ± 1°C). FITC-CD4 (MiltenyiBiotec, BergischGladbach, Germany)-positive T-lymphocytes were detected under fluorescence microscope. The external solution was (in mM): 160 sodium-aspartate, 4.5 KCl, 2 $CaCl_2$, 1 $MgCl_2$ and 5 HEPES, pH 7.4. The pipette solution was (in mM): 145 potassium-aspartate, 2 $MgCl_2$, 10 HEPES, 10 EGTA and 8.5 $CaCl_2$, pH 7.2, with an estimated free Ca^{2+} concentration of 1 μM. The procedures of electrophysiological recordings and data acquisition/analysis for whole-cell recording have been reported previously (Yamazaki *et al.*, 2006). Currents were measured in voltage-clamp mode and induced by ramp depolarization from −120 to +60 mV, 200 ms duration, every 10 s −80 mV holding potential. One micromolar TRAM-34-sensitive current at +40 mV was estimated as the number of channels per cell and slope conductance was calculated at −80 mV (Ghanshani *et al.*, 2000; Beeton *et al.*, 2001).

Flow cytometric analysis

Cell surface markers were analysed with a FACScan flow cytometer (BD LSR, Becton-Dickinson, Franklin Lakes, NJ, USA), acquiring at least 10 000 events, and gated according to forward- and side-scatter. Data were analysed using CellQuest software (Becton-Dickinson). The lymphocyte gate was established by an analysis of the forward angle versus right angle light scatter. The percentage of positively stained cells was determined by comparing the test histograms. Fluorescence-labelled antibodies and the fixation and permeabilization methods used in the present study were described in the Supporting Information.

Cell cycle analysis

For analysis of the cell cycle distribution pattern, isolated ALN T-lymphocytes (10^6 cells) were fixed in ice-cold 70% ethanol overnight. Fixed cells were stained with PBS containing propidium iodide (10 μg·mL^{-1}) and DNase-free RNase (0.1 mg·mL^{-1}). Stained cells were subjected to analysis on a FACScan flow cytometer (Becton-Dickinson) using CellQuest software (Becton-Dickinson).

Chemicals and statistical analysis

Chemicals used are shown in the Supporting Information. Statistical significance between two groups and among multiple groups was evaluated using Student's *t*-tests, Welch's *t*-tests or Tukey's test after *F*-test or ANOVA. Data are presented as the means ± S.E.M.

Results

Enlargement of mice ALNs by Ox sensitization and/or challenge

In the present study, several conditions [the Ox concentration (0.05–3.0%), the sensitization period (5–10 days) and the challenge exposure time (24, 48, 72 h)] were examined to prepare DTH model (Ox+/+), and the adequate experimental condition, which causes the more severe and stable levels of inflammatory symptoms (Supporting Information Fig. S1a, b), ALN enlargements (Figure 1A) and increase in Th-1 cytokine expressions (IL-2 and IFN-γ; Supporting Information

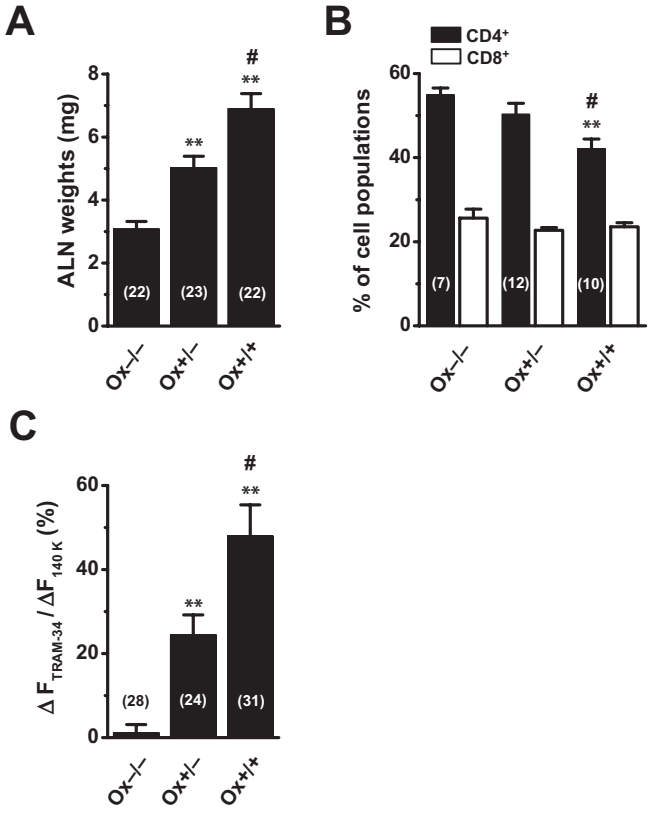

Figure 1

ALN weight in DTH model mice, CD4 and CD8 subset distribution patterns, and depolarization responses induced by $K_{Ca}3.1$ blockade in the ALN T-lymphocytes of DTH model mice: Ox–/–, non-sensitized; Ox+/–, Ox-sensitized control; (Ox+/+), Ox-sensitized and challenged. (A) ALN weights (mg) in Ox–/–, Ox+/– and Ox+/+. (B) CD4 and CD8 subset distribution patterns were analysed by FCM. ALN lymphocytes in Ox–/–, Ox+/– and Ox+/+ were stained with FITC-conjugated anti-CD4 and PE-conjugated anti-CD8 antibodies. The bar graph summarizes the % of each cell population from 7–12 separate experiments: $CD4^+CD8^-$ single-positive ($CD4^+$, closed columns) and $CD4^-CD8^+$ single-positive ($CD8^+$, open columns). (C) Measurement of the TRAM-34 (1 μM)-induced depolarization responses in ALN $CD4^+$ T-lymphocytes using the membrane potential indicator $DiBAC_4(3)$. $K_{Ca}3.1$ was activated by a pre-incubation with ionomycin (0.5 μM) and DCEBIO (10 μM), and then TRAM-34 was applied. Data are shown as the ratio ($\Delta F_{TRAM\text{-}34}/\Delta F_{140\ K}$) of TRAM-34-induced fluorescence change ($\Delta F_{TRAM\text{-}34}$) to 140 mM K^+-induced fluorescence change ($\Delta F_{140\ K}$).

Fig. S1c) in Ox+/+ was determined. In addition, the number of viable ALN lymphocytes determined by the trypan blue dye exclusion assay was increased in the Ox+/– and Ox+/+ mice [3.2 ± 0.5 (n = 9), 5.3 ± 0.8 (n = 7, P < 0.05 vs. Ox–/–), and 10.2 ± 1.0 (n = 10, P < 0.01 vs. Ox–/–; P < 0.05 vs. Ox+/–) ($\times 10^8$ cells per animal)]. Flow cytometry (FCM) showed that there was no significant difference in forward light scatter channel (FSC) distribution (i.e. cell size) in the ALN lymphocytes of the three groups [136.6 ± 1.8 (Ox–/–, n = 5), 133.4 ± 0.6 (Ox+/–, n = 7) and 139.7 ± 2.7 (Ox+/+, n = 6) of the mean fluorescence intensity in FSC, P > 0.05 vs. Ox–/–]. In this study, a viable lymphocyte gate was set on the basis of the FSC and side light scatter channel (SSC; high-FSC/low-SSC) as reported by Chrest *et al*. (1993). In addition, we analysed the frequency of CD3ε, CD4, CD8 (T-lymphocyte antigens) and CD19 (B-lymphocyte antigen) positive cells within the total intact lymphocytes by FCM. Data were expressed as the percentage of lymphocytes of each subpopulation in the total lymphocyte population. In the ALN lymph node lymphocytes in the three groups, approximately 80% of the lymphocytes were the $CD3^+CD19^-$ subpopulation of T-lymphocytes. The percentage of the $CD4^+CD8^-$ ($CD4^+$) subpopulation of ALN T-lymphocytes (closed columns) was slightly, but significantly, decreased in Ox+/+ compared with Ox–/– and Ox+/–; however, the percentage of the $CD4^-CD8^+$ ($CD8^+$) subpopulation of ALN T-lymphocytes (open columns) was unchanged in the three groups (Figure 1B).

Increased depolarization responses induced by K_{Ca}3.1 blockade in ALN T-lymphocytes of Ox+/– and Ox+/+ mice

We next examined the depolarization responses induced by the selective K_{Ca}3.1 blocker TRAM-34 designed by Wulff *et al*. (2000) (IC_{50} = 20 nM) in isolated ALN T-lymphocytes using the membrane potential-sensitive dye, $DiBAC_4(3)$. The TRAM-34 (1 μM)-induced depolarization ($\Delta F_{TRAM\text{-}34}$) was measured after an activating of K_{Ca}3.1 by application of a selective Ca^{2+} ionophore agent, ionomycin (0.5 μM), and the K_{Ca}3.1 activator, DC-EBIO (5,6-dichloro-1-ethyl-1,3-dihydro-2H-benzimidazol-2-one; 10 μM; Supporting Information Fig. S2a). The summarized data are expressed as the ratios ($\Delta F_{TRAM\text{-}34}$ / $\Delta F_{140\ K}$) of $\Delta F_{TRAM\text{-}34}$ to 140 mM high K^+-induced depolarization ($\Delta F_{140\ K}$) (Figure 1C). In the ALN lymphocytes of Ox–/–, the TRAM-34-induced depolarization responses were very small; and significantly larger responses were observed in the ALN lymphocytes of both Ox+/– and Ox+/+ (Figure 1C). Significantly larger depolarization responses were also observed in the ALN lymphocytes of Ox+/+ compared with those of Ox–/– by the application of the K_{Ca}3.1 blocker, ICA-17043 (2,2-bis(4-fluorophenyl)-2-phenylacetamide; 100 nM; Supporting Information Fig. S2b). After measurement of the 140 mM high K^+-induced depolarization, $DiBAC_4(3)$ was washed out for 30 min and the ALN lymphocytes were stained with FITC-CD4. The data were obtained from $CD4^+$ T-lymphocytes alone. We further examined the effects of 1 μM TRAM-34 on the whole-cell membrane; currents were recorded in ALN $CD4^+$ T-lymphocytes of Ox–/– and Ox+/+ by the ramp pulse protocol (Figure 2). In ALN $CD4^+$ T-lymphocytes of Ox+/+, significantly larger levels of current density (Figure 2B), number of channels per cell (Figure 2C) and slope conductance at –80 mV (Figure 2D) were observed.

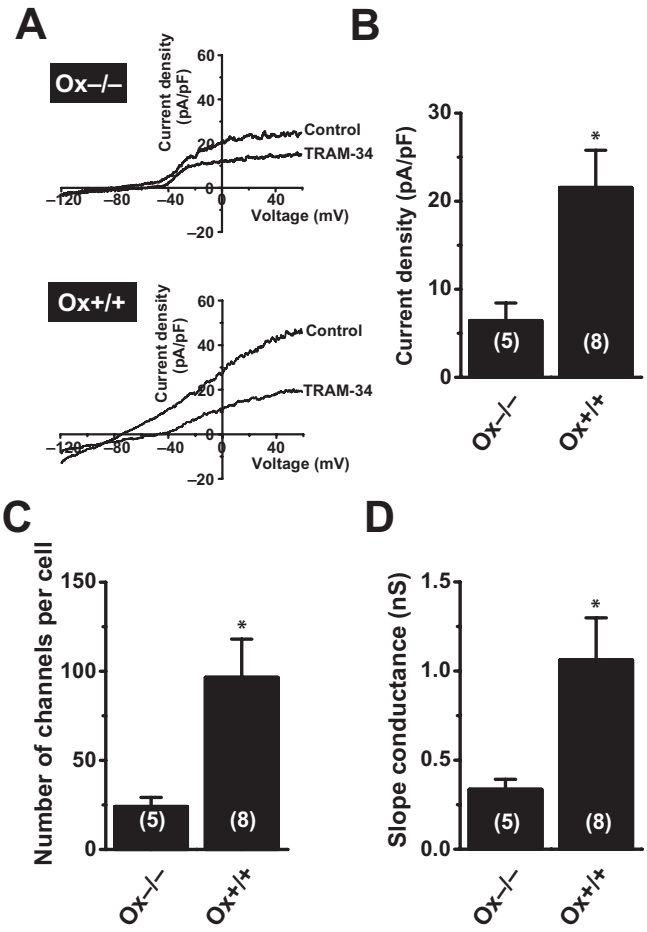

Figure 2

TRAM-34 (1 μM)-sensitive K_{Ca}3.1 K^+ currents in ALN $CD4^+$ T-lymphocytes of Ox–/– and Ox+/+. (A) Current density-voltage relationship for outward K^+ currents in ALN $CD4^+$ T-lymphocytes of Ox–/– and Ox+/+ following treatment with 1 μM TRAM-34. (B) Summarized data for 1 μM TRAM-34-sensitive current density in +40 mV. (C) Summarized data for number of K_{Ca}3.1 channels per cell. (D) Summarized data for the slope conductance (nS) of 1 μM TRAM-34-sensitive currents at –80 mV. The number used for experiments are shown in parentheses. *, P < 0.05 versus Ox–/–.

No significant differences of cell capacitance were observed between ALN $CD4^+$ T-lymphocytes of Ox–/– and Ox+/+ (not shown). We also measured 10 nM margatoxin-sensitive K_V1.3 currents in the presence and absence of 1 μM TRAM-34 in ALN $CD4^+$ T-lymphocytes of Ox+/+, showing no significant differences between them: 22.9 ± 2.3 (n = 6) and 27.3 ± 5.7 pA/pF (n = 4) respectively.

Up-regulation of K_{Ca}3.1 expression in $CD4^+$ ALN T-lymphocytes of Ox+/– and Ox+/+ mice

We examined the transcriptional expression analysis of K_{Ca}3.1 splice variants (K_{Ca}3.1a and K_{Ca}3.1b) in the ALNs of the three groups. Real-time PCR analysis showed that the K_{Ca}3.1a transcript expression was increased in the ALNs of both Ox+/– and Ox+/+ compared with those of Ox–/– (Figure 3A,

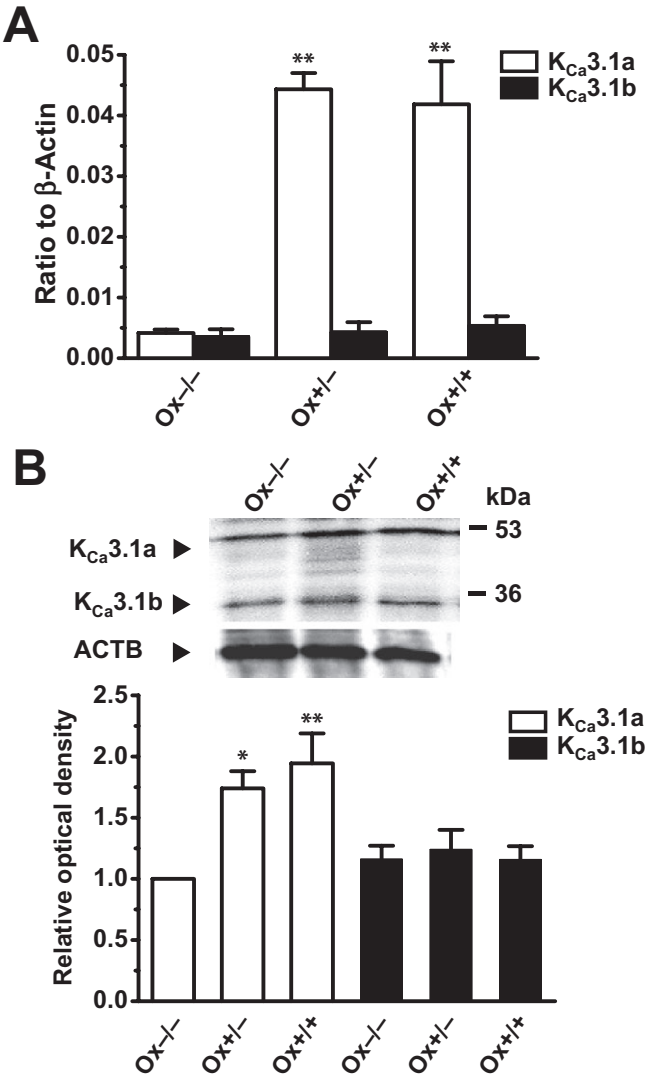

Figure 3

Expression patterns of the $K_{Ca}3.1$ transcripts and proteins in the ALNs of Ox–/–, Ox+/– and Ox+/+. (A) Quantitative, real-time PCR assay for $K_{Ca}3.1$ splice variants in the ALNs of Ox–/–, Ox+/– and Ox+/+: $K_{Ca}3.1a$, open columns; $K_{Ca}3.1b$, closed columns. Results are expressed as the means ± SEM (n = 5 for each). **: $P < 0.01$ versus Ox–/–. (B) Proteins from the plasma membrane fractions were probed by immunoblotting with anti-$K_{Ca}3.1$ and anti-ACTB antibodies respectively. The molecular mass standards are shown in kilodaltons (kDa) at the right side of the upper panel. Arrowheads indicate the migrating positions of $K_{Ca}3.1a$ (50 kDa), $K_{Ca}3.1b$ (25 kDa) and ACTB (40 kDa). The summarized results were obtained as the optical density of each band signal relative to that of the $mK_{Ca}3.1a$ band signal in Ox–/–, and are expressed as the means ± SEM (n = 4 for each). *; **, $P < 0.05$; 0.01 versus Ox–/–.

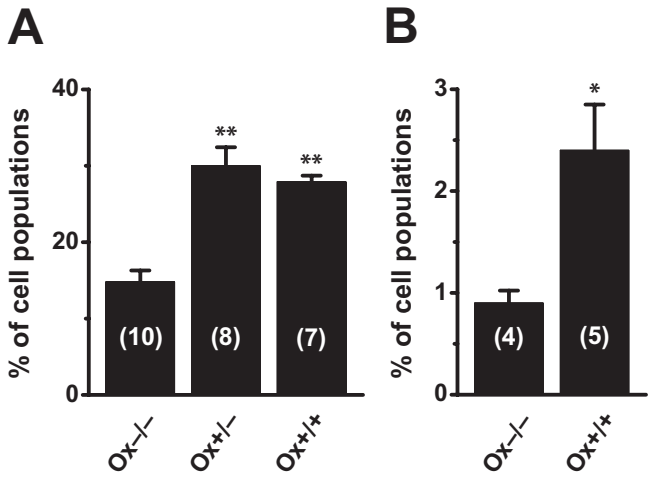

Figure 4

FCM analyses of $K_{Ca}3.1$ and CCR4 expressions in ALN $CD4^+$ T-lymphocytes. (A) ALN lymphocytes in Ox–/–, Ox+/– and Ox+/+ were stained with FITC- CD4 and PE-$K_{Ca}3.1$. The expression level of $K_{Ca}3.1^-$ was determined using a PE-conjugated anti-rabbit IgG antibody. The percentages of the $CD4^+K_{Ca}3.1^+$ subset to the total $CD4^+$ were analysed using CellQuest software (Becton-Dickinson). (B) ALN lymphocytes in Ox–/– and Ox+/+ were double-stained with FITC-CD4 and PE-CCR4. The numbers used for experiments are shown in parentheses. *; **, $P < 0.05$; 0.01 versus Ox–/–.

open columns), whereas no difference in $K_{Ca}3.1b$ transcript expression was found between the ALNs of three groups (Figure 3A, closed columns). Western blot analysis showed an up-regulation of the $K_{Ca}3.1a$ protein in the membrane protein fraction of Ox+/– and Ox+/+ compared with that of Ox–/–, which did not exhibit any effects on the $K_{Ca}3.1b$ protein levels, correlating with the results of the real-time PCR shown in Figure 3A (Ox+/–: $P < 0.05$; Ox+/+: $P < 0.01$ vs. Ox–/–, n = 4 for each) (Figure 3B). The two bands specific for the anti-$K_{Ca}3.1$ antibody, with molecular weights of approximately 50 ($K_{Ca}3.1a$) and 25 ($K_{Ca}3.1b$) kDa, were observed in the plasma membrane protein fractions (Figure 2B, upper panel), and these signals disappeared upon a pre-incubation with excess antigen (not shown).

Subsequently, a fluorescent dual colour dot-plot of FITC-CD4/CD8 versus PE-$K_{Ca}3.1$ in fixed and permeabilized ALN lymphocytes was analysed by FCM. Significantly higher populations of $K_{Ca}3.1^+$ were detected in $CD4^+$ T-lymphocytes of Ox+/– and Ox+/+ than Ox–/– (Figure 4A, Supporting Information Fig. S3a–c), whereas there were no significant changes in $CD8^+$ T-lymphocytes (not shown). The $K_{Ca}3.1^+$ cell population was markedly decreased (to less than 1% of the total) by pre-incubation of the anti-$K_{Ca}3.1$ antibody with excess antigen (Supporting Information Fig. S3d). These results support the conclusion that the significant increase in $K_{Ca}3.1$ activity in $CD4^+$ ALN T-lymphocytes in both Ox+/– and Ox+/+ is due to the increase in the ratio of $K_{Ca}3.1a$ to $K_{Ca}3.1b$.

We further examined whether $K_{Ca}3.1$-expressing ALN $CD4^+$-T-lymphocytes in Ox+/+ are skin-homing, $CLA1^+CCR4^+CCR10^+$ memory T-cells typically observed in DTH (Azam *et al.*, 2007; Wang *et al.*, 2010; Gibhardt *et al.*, 2011). As shown in Figure 4B, $CD4^+CCR4^+$ cells in Ox+/+ were significantly increased compared with those in Ox–/– as reported by Wang *et al.* (2010); however, the percentage of $CD4^+CCR4^+$ cells were less than 3% of ALN $CD4^+$ T-lymphocytes of Ox+/+. In spleen $CD4^+$ T-lymphocytes of Ox+/+, the percentages of $CD4^+CCR4^+$ cells were about 15% of ALN $CD4^+$ T-lymphocytes of Ox+/+ (not shown). These

indicate that the most of $K_{Ca}3.1$-expressing ALN $CD4^+$ T-lymphocytes in Ox+/+ are $CCR4^-$ cells.

Changes in the expression patterns of REST and the AP-1 components in the ALNs of Ox+/– and Ox+/+ mice

It is known that AP-1 (Fos/Jun heterodimers) and REST act as transcriptional factors of $K_{Ca}3.1$ (Ghanshani *et al.*, 2000; Cheong *et al.*, 2005). AP-1 is a heterodimer comprised of Fos (c-Fos, FosB, Fra-1 and Fra-2) and Jun members (c-Jun, JunB and JunD; Jochum *et al.*, 2001). We determined the transcriptional expression of REST, Fos and Jun in the ALNs of the three groups by real-time PCR. Significant down-regulation of the REST transcript was observed in Ox+/– and Ox+/+ mice, but there was no significant difference found in Fos/Jun expression between the ALNs of the three groups (Figure 5A). The expression levels of the other Fos components (c-Fos, FosB and Fra-1) were very low (less than 0.007; not shown). Western blot analysis revealed a down-regulation of the REST proteins in the nuclear protein fraction of Ox+/– and Ox+/+ compared with that of Ox–/–, correlating with the results obtained by real-time PCR shown in Figure 5A ($P < 0.01$ vs. Ox–/–, $n = 4$ for each; Figure 5B). The single band specific for the anti-REST antibody with a molecular weight of approximately 130 kDa (Figure 5B, left panel) disappeared upon pre-incubation with excess antigen (not shown). These findings suggest that the down-regulation of REST, but not AP-1, may contribute to the increase in $K_{Ca}3.1a$ transcription in the ALN $CD4^+$ T-lymphocytes of Ox+/– and Ox+/+.

Effects of the s.c. administration of the $K_{Ca}3.1$ blocker TRAM-34 on ALN enlargement in Ox+/– and Ox+/+ mice

We showed that the s.c. administration of a selective $K_{Ca}3.1$ blocker, TRAM-34 (3 and 10 mg·kg^{-1}, s.c.), significantly inhibits ear swelling in Ox+/+ in a dose-dependent manner (Figure 6A). Similarly, ear plug weights were significantly decreased by the s.c. administration of 10 mg·kg^{-1} TRAM-34 (not shown). Moreover, the ALN weights were significantly decreased by the s.c. administration of 3 and 10 mg·kg^{-1} TRAM-34 (Figure 6B). In parallel, the number of viable ALN lymphocytes determined by the trypan blue dye exclusion assay was significantly decreased by the s.c. administration of TRAM-34 (10 mg·kg^{-1}, s.c.) [vehicle: 9.6 ± 0.5 (n = 12), TRAM-34: 6.3 ± 0.5 (n = 7, $P < 0.01$ vs. vehicle; $\times 10^8$ cells per animal)]. Additionally, FCM showed that there were no significant differences in FSC distribution detected in the ALN lymphocytes of the vehicle control and TRAM-34 (10 mg·kg^{-1}, s.c.)-administered groups. Apoptotic cells were counted using an Annexin V-EGFP apoptosis detection kit (MBL, Nagoya, Japan) by confocal laser microscopy. In the ALN lymphocytes of three groups, almost 100% of the cells were annexin V-negative (not shown). These suggest that decrease in ALN lymphocytes by the s.c. administration of TRAM-34 may be caused by the decrease in cells homing to the ALN rather than cell death within the ALN. A decrease in auricular thickness and the ALN weight was observed when the $K_{Ca}3.1$ blocker, ICA-17043 (3 mg·kg^{-1}, s.c.), was administered to Ox+/+ mice (Supporting Information Fig. S4a, b). The percentages of ALN T-lymphocytes with

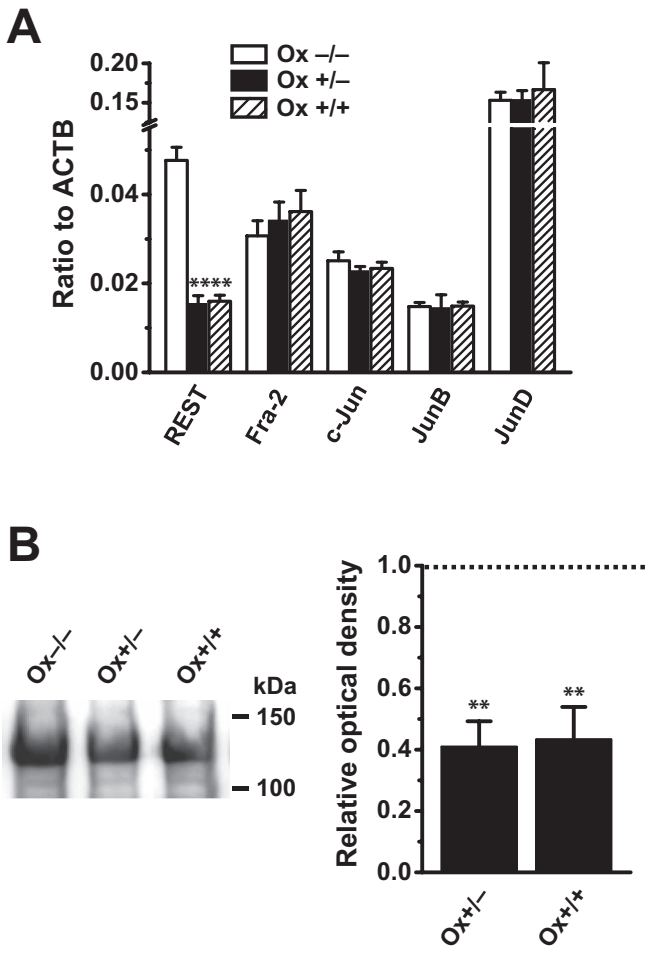

Figure 5

The expression patterns of REST and the AP-1 components (Fra-2, c-Jun, JunB and JunD) in the ALNs of Ox–/–, Ox+/– and Ox+/+. (A) Quantitative, real-time PCR assay for REST, Fra-2, c-Jun, JunB and JunD in the ALNs of Ox–/– (open columns), Ox+/– (closed columns) and Ox+/+ (hatched columns). Results are expressed as the means ± SEM (n = 5 for each). **: $P < 0.01$ versus Ox–/–. (B) Western blot analysis of REST proteins in the ALNs of Ox–/–, Ox+/– and Ox+/+. Proteins from the nuclear fractions were probed by immunoblotting with an anti-REST antibody. The molecular mass standards are shown in kilodaltons (kDa) at the right side of the left panel. The summarized results were obtained as the optical density of each band signal relative to that of the REST band signal in Ox–/–, and expressed as the means ± SEM (n = 4 for each). **, $P < 0.01$ versus Ox–/–.

$CD4^+$ and $CD8^+$ subpopulations were unchanged by the s.c. administration of TRAM-34 (10 mg·kg^{-1}, s.c.), respectively. Measurement of the fluorescence intensity of $DiBAC_4(3)$ using an ARUGUS-HiSCA imaging system showed that the TRAM-34-induced depolarization responses were significantly smaller in the ALN lymphocytes of the TRAM-34 (10 mg·kg^{-1}, s.c.)-administered group than vehicle one (Figure 6C). Also, TRAM-34-sensitive currents (number of channels per cell) and slope conductance at –80 mV were significantly suppressed by the s.c. administration of TRAM-34 (10 mg·kg^{-1}, s.c.; Figure 6D).

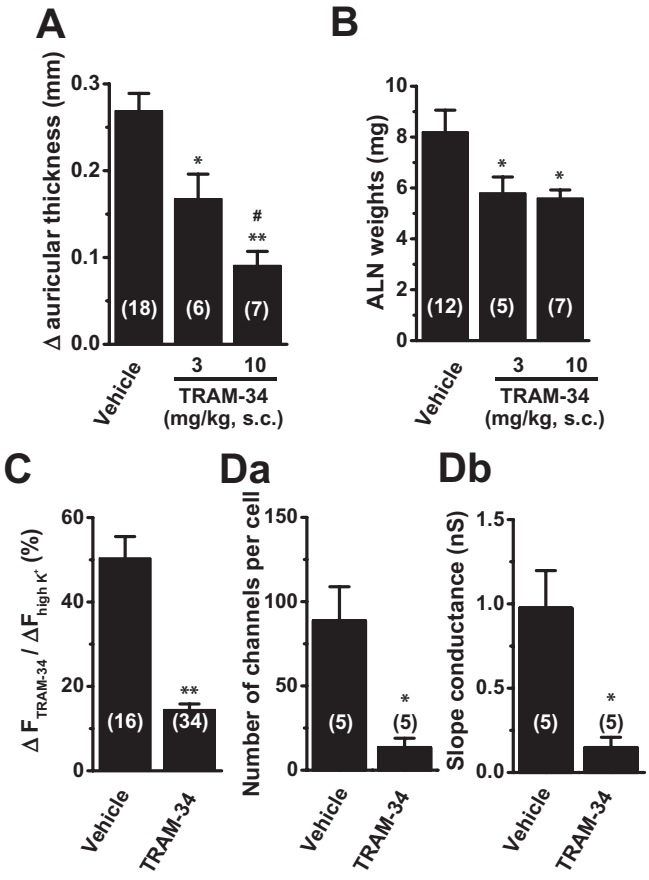

Figure 6

Effects of the s.c. administration of TRAM-34 on auricular thickness and ALN weights in Ox+/+ mice and on TRAM-34-induced depolarization responses and currents in ALN T-lymphocytes of Ox+/+ mice. In Vehicle control, same volume (100 μl) of dimethyl sulfoxide (DMSO) was administered. (A) Effect of the s.c. administration of TRAM-34 on Δauricular thickness (mm) in vehicle control (vehicle) and TRAM-34-administered mice (3 and 10 mg·kg^{-1}, s.c.). (B) Effect of the s.c. administration of TRAM-34 on ALN weights (mg) in three groups. (C) Effect of the s.c. administration of TRAM-34 (10 mg·kg^{-1}, s.c.) on TRAM-34 (1 μM)-induced depolarization responses using a membrane potential indicator, $DiBAC_4(3)$. Data are shown as the ratio ($\Delta F_{TRAM-34}/\Delta F_{140\ K}$) of TRAM-34-induced fluorescence change ($\Delta F_{TRAM-34}$) to 140 mM K^+-induced fluorescence change ($\Delta F_{140\ K}$). $K_{Ca}3.1$ was activated by the pre-incubation with ionomycin (0.5 μM) and DCEBIO (10 μM). (D) Measurements of the number of $K_{Ca}3.1$channels per cell (a) and the slope conductance (nS) of 1 μM TRAM-34-sensitive currents at −80 mV (b) in ALN $CD4^+$ T-lymphocytes of vehicle control (vehicle) and TRAM-34-administered mice (10 mg·kg^{-1}, s.c.) (TRAM-34) by a ramp pulse protocol. Results are expressed as means ± SEM. Numbers used for experiments are shown in parentheses. *; **, $P < 0.05$; 0.01 versus vehicle control; #, $P < 0.05$ versus 3 mg·kg^{-1}, s.c. TRAM-34.

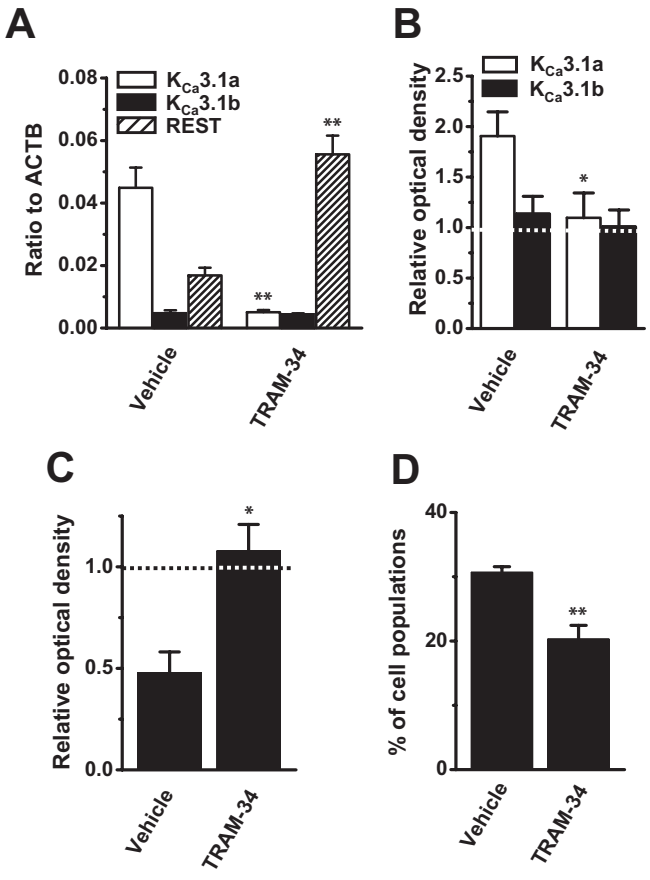

Figure 7

The effects of the s.c. administration of TRAM-34 on the $K_{Ca}3.1$ and REST expression patterns in the ALNs of Ox+/+ and cell population of the $CD4^+K_{Ca}3.1^+$ subset. (A) Quantitative, real-time PCR assay for $K_{Ca}3.1a$ (open columns), $K_{Ca}3.1b$ (closed columns) and REST (hatched columns) in the ALNs of Ox+/+ administered vehicle (dimethyl sulfoxide, DMSO) and TRAM-34 (10 mg·kg^{-1}, s.c.). Results are expressed as the means ± SEM ($n = 5$ for each). **, $P < 0.01$ versus vehicle. (B, C) Western blot analysis of $K_{Ca}3.1$ (B) and REST (C) proteins in the ALNs of Ox+/+ mice administered vehicle and TRAM-34. Proteins from the plasma membrane ($K_{Ca}3.1$) and nuclear (REST) fractions were probed by immunoblotting with anti-$K_{Ca}3.1$ and anti-REST antibodies, respectively. The summarized results were obtained as the optical density of each band signal relative to that of the band signal of the vehicle and are expressed as the means ± SEM ($n = 4$ for each). *, $P < 0.05$ versus vehicle control. (D) FCM analysis of $K_{Ca}3.1$ expression in the $CD4^+$ ALN T-lymphocytes of vehicle- and TRAM-34 (10 mg·kg^{-1}, s.c.)-administered Ox+/+. ALN lymphocytes were double-stained with FITC-CD4 and PE-$K_{Ca}3.1$. Expression level of $K_{Ca}3.1^-$ was determined using a PE-conjugated anti-rabbit IgG antibody. The percentages of the $CD4^+K_{Ca}3.1^+$ subset to the total $CD4^+$ were analyzed using CellQuest software ($n = 5$ for each). *; **, $P <$ 0.05; 0.01 versus vehicle control.

Effects of the s.c. administration of TRAM-34 on $K_{Ca}3.1$ expression and function in the ALN T-lymphocytes of Ox+/– and Ox+/+ mice

The effects of the s.c. administration of TRAM-34 on the expression of $K_{Ca}3.1$ and REST were also examined. As shown in Figure 7A, the transcriptional expression levels of $K_{Ca}3.1a$ and REST were significantly down- and up-regulated by the s.c. administration of TRAM-34 (10 mg·kg^{-1}), respectively ($n =$ 5 for each, $P < 0.01$ vs. vehicle), and were almost identical to those in Ox–/– (see Figures 3A, 5A). Similarly, down-regulation of $K_{Ca}3.1a$ and up-regulation of REST in the ALNs

of Ox+/+ were observed after the s.c. administration of ICA-17043 (3 mg·kg^{-1}, s.c.; Supporting Information Fig. S4c). Western blot analyses showed the s.c. administration of TRAM-34 (10 mg·kg^{-1}) caused down- and up-regulation of K_{Ca}3.1a and REST protein expression in the nuclear protein fractions purified from ALNs of Ox+/+, respectively (n = 4 for each, $P < 0.05$ vs. vehicle; Figure 7B, C), correlating with the results obtained by real-time PCR examination. The optical density of Ox–/– was calculated as 1.0 and the expression of the K_{Ca}3.1a and REST proteins was almost identical to Ox–/– ($P > 0.05$). Significant changes in the expression levels of the K_{Ca}3.1b transcripts and proteins were not observed (Figure 7A, B, closed columns). Of interest, similar suppressive effects on the ALN weight in Ox+/– and the K_{Ca}3.1 function and expression in ALN T-lymphocytes of Ox+/– were observed in Ox+/– mice when TRAM-34 was administered 3 days before Ox challenge (Supporting Information Fig. S5).

Subsequently, a fluorescent dual colour dot-plot of FITC-CD4/CD8 versus PE-K_{Ca}3.1 was analysed by FCM. A significantly lower population of $K_{Ca}3.1^+$ was detected in the CD4$^+$ T-lymphocytes of the TRAM-34 (10 mg·kg^{-1})-administered group than in the vehicle control (Figure 7D), whereas no significant difference in CD8$^+$ was detected (not shown).

Changes in cell cycle progression in ALN T-lymphocytes by the s.c. administration of TRAM-34

We examined the cell cycle status of ALN CD4$^+$ T-lymphocytes of the vehicle and TRAM-34 (10 mg·kg^{-1}, s.c.) groups. Double-staining of ALN lymphocytes with PE-CD4 and PI was performed by FCM. In the CD4$^+$ T-lymphocytes of Ox+/+, pharmacological K_{Ca}3.1 blockade by the administration of TRAM-34 (10 mg·kg^{-1}, s.c.) resulted in cell cycle arrest at the G_0/G_1 phase; in the vehicle control (closed columns, n = 4), the G_0/G_1 results were: 75.5 ± 1.3%, S: 2.0 ± 0.4%, G_2/M: 18.2 ± 0.9%; and in TRAM-34 (10 mg·kg^{-1}, s.c.)-administered group (open columns, n = 5), G_0/G_1 was: 79.8 ± 1.1%, $P < 0.05$, S: 1.4 ± 0.2%, $P > 0.05$, G_2/M: 14.3 ± 0.7%, $P < 0.01$ (Figure 8). In the CD4$^-$ T-lymphocytes of Ox+/+, pharmacological K_{Ca}3.1 blockade by the administration of TRAM-34 (10 mg·kg^{-1}, s.c.) did not result in any significant difference in the cell cycle in the two groups (not shown). These results indicate that the suppression of cell proliferation in CD4$^+$ T-lymphocytes by the administration of TRAM-34 is related to the arrest of the G_1/S and G_2/M transitions during cell cycle progression.

Up-regulation of the K_{Ca}3.1positive regulator transcripts, phosphoinositide-3-kinase, class 2, β polypeptide (PI3K-C2β) and nucleoside diphosphate kinase B (NDPK-B) in ALN CD4$^+$ T-lymphocytes of Ox+/+

K_{Ca}3.1 activity was significantly higher in ALN CD4$^+$ T-lymphocytes of Ox+/+ than Ox+/– (Figures 1C, 2), but the K_{Ca}3.1 gene and protein expression patterns were almost identical in the ALN CD4$^+$ T-lymphocytes of the two groups (Figures 3, 4). Therefore, the transcriptional expression patterns of the positive regulators (PI3K-C2β, NDPK-B) and negative regulators (phosphatidylinositol 3-phosphate phosphatase myotubularin-related protein 6; MTMR6, phosphohistidine phosphatase 1; PHPT1) of K_{Ca}3.1 were compared between Ox+/– and Ox+/+. In the isolated ALN CD4$^+$ T-lymphocytes of Ox+/+, transcriptional expression levels of both PI3K-C2β and NDPK-B were significantly higher than in those of Ox+/– (Figure 9Aa, Ba). The s.c. administration of TRAM-34 (10 mg·kg^{-1}) in Ox+/+ elicited a significant down-regulation of the their transcripts (Figure 9Ab, Bb). On the other hand, there were no significant differences in the MTMR6 and PHPT1 expression levels between Ox+/– and Ox+/+ (not shown). These findings suggest that up-regulation of PI3K-C2β and NDPK-B may be responsible for the higher K_{Ca}3.1 activity in the ALN CD4$^+$ T-lymphocytes of Ox+/+ compared with those of Ox+/–.

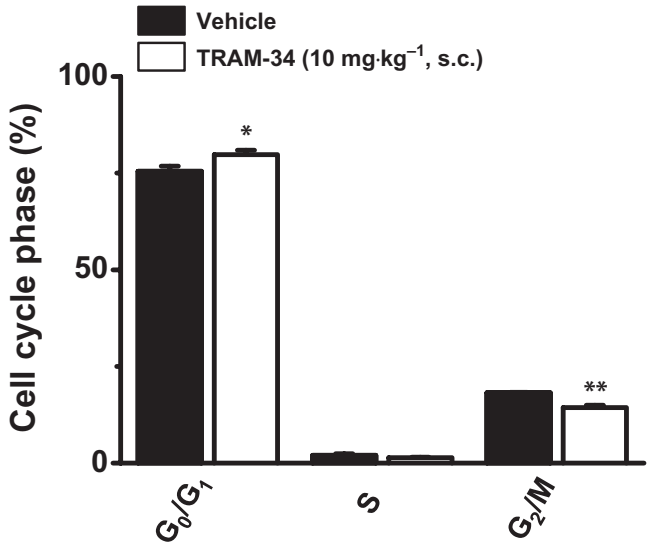

Figure 8

The effect of *in vivo* TRAM-34 administration on the percentage of the phase populations in the cell cycle of the ALN CD4$^+$ T-lymphocytes in Ox+/+. Cell cycle progression was monitored by the detection of DNA content using FCM analysis. The total ALN lymphocytes were isolated, fixed and permeabilized. DNA was labelled with propidium iodide. The cell cycle distribution was analysed by CellQuest software and depicted in a histogram. The data on the cell cycle distribution in the ALN CD4$^+$ T-lymphocytes of the vehicle- (n = 4) and TRAM-34 (10 mg·kg^{-1}, s.c., n = 5)-administered Ox+/+ were summarized and expressed as percentages of the G_0/G_1, S, G_2/M phases (means ± SEM). *; **, $P < 0.05$; 0.01 versus vehicle control.

Discussion and conclusions

The main findings in the present study are as follows: (i) CD4$^+$ T-lymphocyte proliferation is stimulated by up-regulation of K_{Ca}3.1a expression in ALNs of a skin contact chemical sensitizer (Ox)-induced DTH model mice; (ii) the transcriptional regulation of T-lymphocyte K_{Ca}3.1 is carried out by REST, but not AP-1; and (iii) the prevention of the up-regulation of K_{Ca}3.1 and down-regulation of REST as well as cell-cycle progression was achieved by pharmacological blockade of K_{Ca}3.1 in the CD4$^+$ ALN T-lymphocytes of DTH model mice. Similar to the inhibition of ear swelling in the

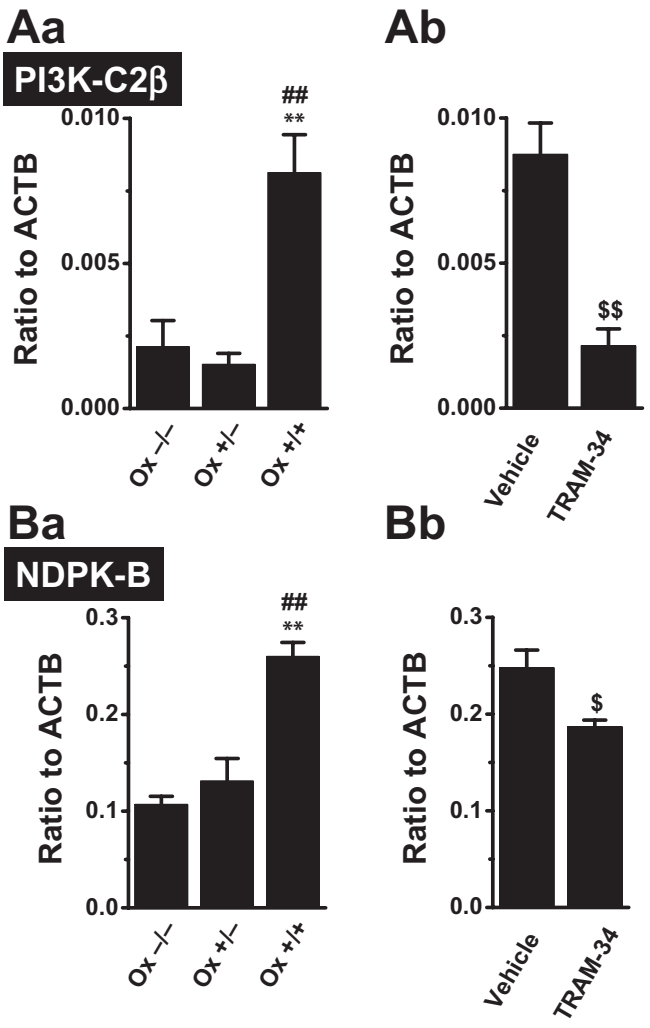

Figure 9

Expressions of PI3K-C2β and NDPK-B transcripts in ALN $CD4^+$ T-lymphocytes of Ox–/–, Ox+/– and Ox+/+, and the effect of the administration of TRAM-34. (Aa, Ba) Quantitative, real-time PCR assay for PI3K-C2β (Aa) and NDPK-B (Ba) in ALN $CD4^+$ T-lymphocytes of Ox–/–, Ox+/– and Ox+/+. The results are expressed as the means ± SEM (n = 5 for each). **, $P < 0.01$ versus Ox–/–. $^{\#\#}$, $P < 0.01$ versus Ox+/–. (Ab, Bb) Quantitative, real-time PCR assay for PI3K-C2β (Ab) and NDPK-B (Bb) in ALN $CD4^+$ T-lymphocytes of the vehicle- (n = 4) and TRAM-34 (10 mg·kg^{-1}, s.c., n = 4)-administered Ox+/+. Results are expressed as the means ± SEM (n = 5 for each). $^{\$\$}$, $P < 0.01$ versus vehicle control.

Ox-induced DTH model by the $K_{Ca}3.1$ blocker, clotrimazole (Pegoraro *et al.*, 2009), which has several anti-proliferative effects other than channel blocking (Aktas *et al.*, 1998; Zhang *et al.*, 2002; Cruse *et al.*, 2006), the present study showed that ear swelling in the Ox-induced DTH model was inhibited by the s.c. administration of the selective and potent $K_{Ca}3.1$ blockers TRAM-34 (Figure 5A) and ICA-17043 (Supporting Information Fig. S4a).

DTH is an inflammatory response mediated by effecter memory T (T_{EM}) cells. In chronically activated T_{EM} cells, the voltage-gated K^+ channel subtype $K_V1.3$ is predominantly expressed, and the $K_V1.3$ blockade suppressed the motility and activation of T_{EM} cells in inflamed tissue of animal models of DTH and the other immune disease (Matheu *et al.*, 2008; Pennington *et al.*, 2009; Gocke *et al.*, 2012; Tarcha *et al.*, 2012) and human DTH (Beeton and Chandy, 2005; Varga *et al.*, 2012). In ALN $CD4^+$ T-lymphocytes of Ox+/+, significant increase in $K_V1.3$ expression and activity was observed (Supporting Information Fig. S6). Wang *et al.* (2010) have studied T-cells with the skin homing receptor CCR4 in lymph nodes of Ox-induced DTH model, and suggested that CLA^+CCR4^+ cells within $CD4^+$ cell population are under 5% in Ox+/+. Consistent with this, the present study showed that $CCR4^+$ cells within $CD4^+$ cell population in Ox+/+ ALN were less than 3% (Figure 4B). Figure 4A showed that 30% cells within $CD4^+$ cell populations were $K_{Ca}3.1^+$ cells, indicating that most of $CD4^+K_{Ca}3.1^+$ cells are $CCR4^-$ cells.

Increases in local lymph node weight are mainly attributed to T-cell proliferation, with common immunological patterns of Th1 cell reactivity (Chipinda *et al.*, 2009; Ahlfors and Lyberg, 2010). Similar to the results by Ahlfors and Lyberg (2010), up-regulation of IL-2 and IFN-γ transcripts in ALN T-lymphocytes of Ox+/+ was observed in the present study (Supporting Information Fig. S1c). Di *et al.* (2010a) showed that Ca^{2+} influx via CRAC channels by $K_{Ca}3.1$ activation is essential for IL-2 production in T-lymphocytes, and that $K_{Ca}3.1$ activity is markedly increased following differentiation into Th1 cells. Our study showed that the increase in $K_{Ca}3.1$ activity was observed in ALN T-lymphocytes of Ox+/– and Ox+/+ having the cell population of $CD4^+$ (Figure 1C). Recently, we have identified the dominant-negative isoform of $K_{Ca}3.1$, $K_{Ca}3.1b$, from lymphoid tissues, and showed that an up-regulation of $K_{Ca}3.1b$ induced the inhibition of cell proliferation in mice thymocytes (Ohya *et al.*, 2011b). Alternative splicing patterns of ion channels are involved in the pathogenesis of several diseases (Murthy *et al.*, 2008; Lioa *et al.*, 2009). For instance, a shorter isoform of the small-conductance Ca^{2+}-activated K^+ channel, $K_{Ca}2.2$, which has no functional channel activity, is implicated in the pathogenesis of Alzheimer's disease (Murthy *et al.*, 2008). Therefore, down-regulation of $K_{Ca}3.1b$, in addition to an up-regulation of $K_{Ca}3.1a$, may be responsible for the increase in $K_{Ca}3.1$ activity in ALN $CD4^+$ T-lymphocytes of Ox+/– and Ox+/+ (Figure 1C). However, as shown in the results of the $K_{Ca}3.1$ expression analyses in Figure 2, up-regulation of $K_{Ca}3.1a$, but not down-regulation of $K_{Ca}3.1b$, is in fact responsible for the increase in $K_{Ca}3.1$ activity in ALN $CD4^+$ T-lymphocytes of Ox+/– and Ox+/+.

In addition, up-regulation of $K_{Ca}3.1a$ occurs in conjunction with the down-regulation of REST in ALN $CD4^+$ T-lymphocytes in DTH model (Figure 3). This up-regulation of $K_{Ca}3.1$ in conjunction with the down-regulation of REST leads to the proliferative phenotype in both vascular SMCs (Cheong *et al.*, 2005) and implanted urogenital sinus cells of a stromal hyperplasia benign prostatic hyperplasia model (Ohya *et al.*, 2011a), respectively. In T-lymphocytes, it is known that up-regulation of $K_{Ca}3.1$ in conjunction with up-regulation of AP-1 (Fos/Jun) leads to T-cell activation (Ghanshani *et al.*, 2000). To the best of our knowledge, this is the first report of an up-regulation of $K_{Ca}3.1$ in conjunction with down-regulation of REST in T-lymphocytes. Tharp *et al.* (2008) have suggested that the initial hyperpolarization

attributable to $K_{Ca}3.1$ activity may drive the down-regulation of REST in dedifferentiated vascular SMCs. In the present study, the administration of TRAM-34 and ICA-17043 prevented a down-regulation of REST in the ALN $CD4^+$ T-lymphocytes of Ox+/– and Ox+/+ (Figure 6, Supporting Information Fig. S4c). To show the negative correlation between $K_{Ca}3.1$ and REST protein expression in $CD4^+$ T-lymphocytes, we performed a fluorescent dual colour dot-plot of Alexa Fluor® 488 (Invitrogen, Carlsbad, CA, USA)-$K_{Ca}3.1$ versus Alexa Fluor (Invitrogen) 594-REST in fixed and permeabilized $CD4^+$ T-lymphocytes by FCM. However no signals specific for REST were detectable because the non-specific signals for REST were too high (not shown). Taken together, $K_{Ca}3.1$ activation may be important for the down-regulation of REST in Ox-sensitization and/or -challenge. Of interest, the decrease in the ALN weight and $K_{Ca}3.1$ activity in ALN T-lymphocytes, which was achieved by the prevention of up-regulation of $K_{Ca}3.1$ expression in conjunction with down-regulation of REST, were also observed in Ox+/– when TRAM-34 (10 $mg \cdot kg^{-1}$, s.c.) was administered 3 days after sensitization (Supporting Information Fig. S5). Pharmacological approaches such as the s.c. administration of TRAM-34 corroborated the proposed concept that pharmacological blockade of $K_{Ca}3.1$ is effective for prophylactic treatment in the pathogenesis of allergic diseases such as DTH.

For the therapeutic usage of drugs, it is important to monitor the changes in the pattern of gene expression of the drug targets (Iskar *et al*., 2010). The present study showed that the pharmacological blockade of $K_{Ca}3.1$ activity by TRAM-34 and ICA-17034 induced a down-regulation of $K_{Ca}3.1a$ in conjunction with an up-regulation of REST (Figure 6, Supporting Information Fig. S4c) without changes in the expressions of $K_{Ca}3.1b$ (Figure 6A, B). Tharp *et al*. (2006; 2008) have shown that up-regulation of the $K_{Ca}3.1$ gene can be regulated at the epigenetic level, and that pharmacological blockade of $K_{Ca}3.1$ may induce the epigenetic silencing of the $K_{Ca}3.1$ gene. Recently, Lu *et al*. (2011) have found the microRNA strongly associating with the severity of DTH. It remains unclear whether epigenetic and/or microRNA regulation of $K_{Ca}3.1a$ exists in ALN $CD4^+$ T-lymphocytes by the pharmacological blockade of $K_{Ca}3.1$. Furthermore, blockade of ion channel activity is strongly associated with cell-cycle arrest; and $K_{Ca}3.1$ activity is involved in the transition to the S phase and entry to the G_2/M phase in cancer cells (Chou *et al*., 2008; Becchetti, 2011). In renal fibroblasts and 3T3-L1 pre-adipocytes, both pharmacological blockade and gene silencing of $K_{Ca}3.1$ have caused an accumulation of cells at the G_0/G_1 phase (Grgic *et al*., 2009b; Zhang *et al*., 2012). The present study showed that the s.c. administration of TRAM-34 suppressed the cell cycle progression through both the G_1/S and G_2/M transitions in ALN $CD4^+$ T-lymphocytes of Ox+/+ (Figure 8). Up-regulation of $K_{Ca}3.1$ may promote cell-cycle progression in ALN $CD4^+$ T-lymphocytes in DTH and induce abnormal T-cell function.

In ALN $CD4^+$ T-lymphocytes, $K_{Ca}3.1$ activity was enhanced after Ox challenge (Figure 1C) without any significant changes in the $K_{Ca}3.1$ expression level between ALN $CD4^+$ T-lymphocytes of Ox+/- and Ox+/+ (Figures 2, 3). It has been reported that PI3K-C2β and NDPK-B play important roles for T-cell activation and immunological synapse formation (Srivastava *et al*., 2009; Di *et al*., 2010b). Of four regulators of $K_{Ca}3.1$ activity in $CD4^+$ T-lymphocytes, the transcriptional expression levels of the positive regulators, PI3K-C2β and NDPK-B, were significantly up-regulated in ALN $CD4^+$ T-lymphocytes after Ox challenge (Figure 9Aa, Ba), suggesting that PI3K-C2β and NDPK-B may dynamically regulate the $K_{Ca}3.1$ activity in ALN $CD4^+$ T-lymphocytes; and that the enhancement of $K_{Ca}3.1$ activity by up-regulation of them in ALN $CD4^+$ T-lymphocytes may be in part associated with the infiltration of $CD4^+$ T-lymphocytes into the inflamed skin of Ox+/+.

In conclusion, this study provides evidence that $K_{Ca}3.1$ plays a crucial role in the ALN increase induced by $CD4^+$ T-lymphocyte proliferation during the development of DTH. It was demonstrated that REST regulates $K_{Ca}3.1$ expression in T-lymphocytes. $K_{Ca}3.1$-induced hyperpolarization can drive the expression of $K_{Ca}3.1a$ in a positive-feedback manner. Pharmacological blockade of $K_{Ca}3.1$ inhibited the expression of $K_{Ca}3.1a$ and increased the expression of REST, and also prevented cell cycle progression in ALN $CD4^+$ T-lymphocytes, resulting in quiescent T-cell subsets. Clinical trials on the effects of the specific $K_{Ca}3.1$ blocker ICA-17043 (Senicapoc, Neusentis, Cambridge, UK) in sickle cell anaemia have reported a lack of evident adverse effects, suggesting specific $K_{Ca}3.1$ blockers have therapeutic potential in human diseases. These findings should prove to be useful information for the prevention and treatment of allergic diseases such as DTH.

Acknowledgements

This work was supported by Grant-in-Aid for Scientific Research (C) for the Japan Society for the Promotion of Science (JSPS) (21590098) (S.O.), the Salt Science Research Foundation (No.10C6) (S.O.), Takeda Science Foundation (S.O.), the Suzuken Memorial Foundation (S.O.), Grant-in-Aid for Scientific Research (B) from JSPS (20390027) (Y.I.) and Grant-in Aid for Scientific Research on Priority Areas: 'Transportsome' from the Ministry of Education, Culture, Sports, Science and Technology (MEXT) (20056027) (Y.I.). Pacific Edit reviewed the manuscript prior to submission.

Conflict of interest

The authors declare they have no conflicts of interest.

References

Ahlfors EE, Lyberg T (2010). Kinetics of local tissue and regional lymph node IL-2 and IFN-γ responses in experimental oral mucosa and skin contact sensitivity in mice. Scand J Immunol 72: 8–14.

Aktas H, Fluckiger R, Acosta JA, Savage JM, Palakurthi SS, Halperin JA (1998). Depletion of intracellular Ca^{2+} stores, phosphorylation of eIF2alpha, and sustained inhibition of translation initiation mediate the anticancer effects of clotrimazole. Proc Natl Acad Sci U S A 95: 8280–8285.

Azam P, Sankaranarayanan A, Homerick D, Griffey S, Hulff H (2007). Targeting effector memory T cells with the small molecule Kv1.3 blocker PAP-1 suppresses allergic contact dermatitis. J Invest Dermatol 127: 1419–1429.

Becchetti A (2011). Ion channels and transporters in cancer. 1. Ion channels and cell proliferation in cancer. Am J Physiol Cell Physiol 301: C255–C265.

Beeton C, Chandy KG (2005). Potassium channels, memory T cells, and multiple sclerosis. Neuroscientist 11: 550–562.

Beeton C, Wulff H, Barbaria J, Clot-Faybesse O, Pennington M, Bernard D *et al.* (2001). Selective blockade of T lymphocyte K^+ channels ameliorates experimental autoimmune encephalomyelitis, a model for multiple sclerosis. Proc Natl Acad Sci U S A 98: 13942–13947.

Cahalan MD, Chandy KG (2009). The functional network of ion channels in T lymphocytes. Immunol Rev 231: 59–87.

Chandy KG, Wulff H, Beeton C, Pennington M, Gutman GA, Cahalan MD (2004). K^+ channels as targets for specific immunomodulation. Trends Pharmacol Sci 25: 280–289.

Chantome A, Girault A, Potier M, Collin C, Vaudin P, Pages JC *et al.* (2009). $K_{Ca}2.3$ channel-dependent hyperpolarization increases melanoma cell motility. Exp Cell Res 315: 3620–3630.

Cheong A, Bingham AJ, Li J, Kumar B, Sukumar P, Munsch C *et al.* (2005). Downregulated REST transcription factor is a switch enabling critical potassium channel expression and cell proliferation. Mol Cell 20: 45–52.

Chipinda I, Anderson SE, Butterworth LF, Beezhold D, Siegel PD (2009). Increased cell proliferation in spleen and lymph nodes peripheral to contact allergen application site. Toxicology 257: 113–116.

Chou CC, Lunn CA, Murgolo NJ (2008). KCa3.1: target and marker for cancer, autoimmune disorder and vascular inflammation. Expert Rev Mol Diagn 8: 179–187.

Chrest FJ, Buchholz MA, Kim YH, Kwon TK, Nordin AA (1993). Identification and quantitation of apoptotic cells following anti-CD3 activation of murine G_0 T cells. Cytometry 14: 883–890.

Cruse G, Duffy SM, Brightling CE, Bradding P (2006). Functional $K_{Ca}3.1$ K^+ channels are required for human lung mast cell migration. Thorax 61: 880–885.

Di L, Srivastava S, Zhdanova O, Ding Y, Li Z, Wulff H *et al.* (2010a). Inhibition of the K^+ channel $K_{Ca}3.1$ ameliorates T cell-mediated colitis. Proc Natl Acad Sci U S A 107: 1541–1546.

Di L, Srivastava S, Zhdanova O, Sun Y, Li Z, Skolnik EY (2010b). Nucleoside diphosphate kinase B knock-out mice have impaired activation of the K^+ channel $K_{Ca}3.1$, resulting in defective T cell activation. J Biol Chem 285: 38765–38771.

Evans DP, Hossack M, Thomson DS (1971). Inhibition of contact sensitivity in the mouse by topical application of corticosteroids. Br J Pharmacol 43: 403–408.

Funabashi K, Fujii M, Yamamura H, Ohya S, Imaizumi Y (2010). Contribution of chloride channel conductance to the regulation of resting membrane potential in chondrocyte. J Pharmacol Sci 113: 94–99.

Ghanshani S, Wulff H, Miller MJ, Rohm H, Neben A, Gutman GA *et al.* (2000). Up-regulation of the $IK_{Ca}1$ potassium channel during T-cell activation. Molecular mechanism and functional consequences. J Biol Chem 275: 37137–37149.

Gibhardt T, Whitney PG, Zaid A, Mackay LK, Brooks AG, Heath WR *et al.* (2011). Different patterns of peripheral migration by memory $CD4^+$ and $CD8^+$ T cells. Nature 477: 216–219.

Gocke AR, Lebson LA, Grishkan IV, Nguyen HM, Whartenby KA, Chandy KG *et al.* (2012). Kv1.3 deletion biases T cells toward an immunoregulatory phenotype and renders mice resistance to autoimmune encephalomyelitis. J Immunol 188: 5877–5886.

Gopalakrishnan V (2009). REST and RESTless: in stem cells and beyond. Future Neurol 4: 317–329.

Grgic I, Kaistha BP, Paschen S, Kaistha A, Busch C, Si H *et al.* (2009a). Disruption of the Gardos channel ($K_{Ca}3.1$) in mice causes subtle erythrocyte macrocytosis and progressive splenomegaly. Pflügers Arch 458: 291–302.

Grgic I, Kiss E, Kaistha BP, Busch C, Kloss M, Sautter J *et al.* (2009b). Renal fibroblast is attenuated by targeted disruption of $K_{Ca}3.1$ potassium channels. Proc Natl Acad Sci U S A 106: 14518–14523.

Iskar M, Campillos M, Kuhn M, Jensen LJ, Noort VV, Bork P (2010). Drug-induced regulation of target expression. PLoS Comput Biol 9: e1000925.

Jensen BS, Strobaek D, Olesen SP, Christophersen P (2001). The Ca^{2+}-activated K^+ channel of intermediate conductance: a molecular target for novel treatments? Curr Drug Targets 2: 401–422.

Jochum W, Passegue E, Wagner EF (2001). AP-1 in mouse development and tumorigenesis. Oncogene 20: 2401–2412.

Köhler R, Wulff H, Eichler I, Kneifel M, Neumann D, Knorr S *et al.* (2003). Blockade of the intermediate-conductance calcium-activated potassium channel as a new therapeutic strategy for restenosis. Circulation 108: 1119–1125.

Lioa P, Ahang HY, Soong TW (2009). Alternative splicing of voltage-gated calcium channels: from molecular biology to disease. Pflügers Arch 458: 481–487.

Lu TX, Hartner J, Lim EJ, Fabry V, Mingler MK, Cole ET *et al.* (2011). MicroRNA-21 limits in vivo immune response-mediated activation of the IL-12/IFN-gamma pathway, Th1 polarization, and the severity of delayed-type hypersensitivity. J Immunol 187: 3362–3373.

Matheu MP, Beeton C, Garcia A, Chi V, Rangaraju S, Safrina O *et al.* (2008). Imaging of effector memory T cells during a delayed-type hypersensitivity reaction and suppression by $K_V1.3$ channel block. Immunity 29: 602–614.

Murthy SR, Teodorescu G, Nijholt IM, Dolga AM, Grissmer S, Spiess J *et al.* (2008). Identification and characterization of a novel, shorter isoform of the small conductance Ca^{2+}-activated K^+ channel SK2. J Neurochem 106: 2312–2321.

Nicolaou SA, Neumeier L, Peng Y, Devor DC, Conforti L (2007). The Ca^{2+}-activated K^+ channel $K_{Ca}3.1$ compartmentalizes in the immunological synapse of human T lymphocytes. Am Physiol Cell Physiol 292: C1431–C1439.

Ohya S, Kuwata Y, Sakamoto K, Muraki K, Imaizumi Y (2005). Cardioprotective effects of estradiol include the activation of large-conductance Ca^{2+}-activated K^+ channels in cardiac mitochondria. Am J Physiol Heart Circ Physiol 289: H1635–H1642.

Ohya S, Niwa S, Kojima Y, Sasaki S, Sakuragi M, Kohri K *et al.* (2011a). Intermediate-conductance Ca^{2+}-activated K^+ channel, $K_{Ca}3.1$, as a novel therapeutic target of benign prostatic hyperplasia. J Pharmacol Exp Ther 338: 528–536.

Ohya S, Niwa S, Yanagi A, Fukuyo Y, Yamamura H, Imaizumi Y (2011b). Dominant-negative, spliced variants of the intermediate-conductance Ca^{2+}-activated K^+ channel, $K_{Ca}3.1$ in lymphoid cells. J Biol Chem 286: 16940–16952.

Pegoraro S, Lang M, Dreker T, Kraus J, Hamm S, Meere C *et al.* (2009). Inhibitors of potassium channels $K_V1.3$ and IK-1 as immunosuppressants. Bioorg Med Chem Lett 19: 2299–2304.

Pennington MW, Beeton C, Galea CA, Smith BJ, Chi V, Monaghan KP *et al.* (2009). Engineering a stable and selective peptide blocker of the Kv1.3 channel in T lymphocytes. Mol Pharmacol 75: 762–773.

Shepherd MC, Duffy SM, Harris T, Cruse G, Schuliga M, Brightling CE *et al.* (2007). $K_{Ca}3.1$ Ca^{2+} activated K^+ channels regulate human airway smooth muscle proliferation. Am J Respir Cell Mol Biol 37: 525–531.

Srivastava S, Li Z, Lin L, Liu G, Ko K, Coetzee WA *et al.* (2005). The phosphatidylinositol 3-phosphate phosphatase myotubularin-related protein 6 (MTMR6) is a negative regulator of the Ca^{2+}-activated K^+ channel $K_{Ca}3.1$. Mol Cell Biol 25: 3630–3638.

Srivastava S, Li A, Ko K, Choudhury P, Albaqumi M, Johnson AK *et al.* (2006). Histidine phosphorylation of the potassium channel $K_{Ca}3.1$ by nucleoside diphosphate kinase B is required for activation of $K_{Ca}3.1$ and CD4 T cells. Mol Cell 24: 665–675.

Srivastava S, Zhdanova O, Di L, Li Z, Albaqumi M, Wulff H *et al.* (2008). Protein histidine phosphatase 1 negatively regulates CD4 T cells by inhibiting the K^+ channel $K_{Ca}3.1$. Proc Natl Acad Sci U S A 105: 14442–14446.

Srivastava S, Di L, Zhdanova O, Li Z, Vardhana S, Wan Q *et al.* (2009). The class II phosphatidylinositol 3 kinase C2β is required for the activation of the K^+ channel $K_{Ca}3.1$ and CD4 T-cells. Mol Biol 20: 3783–3791.

Tarcha EJ, Chi V, Muñoz-Elías EJ, Bailey D, Londono LM, Upadhyay SK *et al.* (2012). Durable pharmacological responses from the peptide ShK-186, a specific Kv1.3 channel inhibitor that suppresses T cell mediators of autoimmune disease. J Pharmacol Exp Ther 342: 642–653.

Tharp DL, Wamhoff BR, Turk JR, Bowles DK (2006). Upregulation of intermediate-conductance Ca^{2+}-activated K^+ channel ($IK_{Ca}1$) mediates phenotypic modulation of coronary smooth muscles. Am J Physiol Heart Circ Physiol 291: H2493–H2503.

Tharp DL, Wamhoff BR, Wulff H, Raman G, Cheong A, Bowles DK (2008). Local delivery of the $K_{Ca}3.1$ blocker, TRAM-34, prevents acute angioplasty-induced coronary smooth muscle phenotypic modulation and limits stenosis. Arterioscler Thromb Vasc Biol 28: 1084–1089.

Varga Z, Gurrola-Briones G, Papp F, Rodríguez de la Vega RC, Pedraza-Alva G, Tajhya RB *et al.* (2012). Vm24, a natural immunosuppressive peptide, potently and selectively blocks Kv1.3 potassium channels of human T cells. Mol Pharmacol 82: 372–382.

Wang X, Fujita M, Prado R, Tousson A, Hsu HC, Schottelius A *et al.* (2010). Visualizing $CD4^+$ T-cell migration into inflamed skin and its inhibition by CCR4/CCR10 blockades using in vivo imaging model. Br J Dermatol 162: 487–496.

Wulff H, Miller MJ, Hänsel W, Grissmer S, Cahalan MD, Chandy KG (2000). Design of a potent and selective inhibitor of the intermediate-conductance Ca^{2+}-activated K^+ channel, *IKCa1*: a potential immunosuppressant. Proc Natl Acad Sci U S A 97: 8151–8156.

Yamazaki D, Aoyama M, Ohya S, Muraki K, Asai K, Imaizumi Y (2006). Novel functions of small conductance Ca^{2+} activated K^+ channel in the promotion of cell proliferation by ATP in brain endothelial cells. J Biol Chem 281: 38430–38439.

Zhang W, Ramamoorthy Y, Lilicarslan T, Nolte H, Tydale RF, Sellers EM (2002). Inhibition of cytochromes P450 by antifungal imidazole derivatives. Drug Metab Dispos 30: 214–318.

Zhang XH, Zhang YY, Sun HY, Jin MW, Li GR (2012). Functional ion channels and cell proliferation in 3T3-L1 preadipocytes. J Cell Physiol 227: 1972–1979.

Supporting information

Additional Supporting Information may be found in the online version of this article at the publisher's web-site:

Figure S1 Auricular thickness, ear plug weight, and cytokine expression in Ox–/–, Ox+/– and Ox+/+. A: Auricular thickness in Ox–/–, Ox+/– and Ox+/+. B: Ear plug weight (mg) in Ox–/–, Ox+/– and Ox+/+. The numbers of used for the experiments are shown in parentheses. C: Transcriptional expression of interleukin-2 (IL-2) (a) and interferon (INF)-γ (b) in ALN $CD4^+$ T-lymphocytes of Ox–/–, Ox+/– and Ox+/+ (n = 5 for each). The results are expressed as the means ± SEM. *, **: $P < 0.05$, 0.01 versus Ox–/–; ##: $P < 0.01$ versus Ox+/–.

Figure S2 The membrane potential was hyperpolarized by pre-incubation with ionomycin (0.5 μM) and DCEBIO (10 μM), and then the TRAM-34 (1 μM) (A) and ICA-17043 (100 nM) (Ba)-induced depolarization responses ($F_{TRAM-34}$ and $F_{ICA-17043}$) were measured in the $CD4^+$ T-lymphocytes of the Ox+/+ mice using $DiBAC_4(3)$. At the end-point of each experiment, 140 mM K^+-induced depolarization ($F_{140\ K}$) was measured. Measurement of the fluorescence intensity of $DiBAC_4(3)$ was performed using an ARUGUS-HiSCA imaging system. Bb: Data are shown as the ratio ($\Delta F_{ICA-17043}/\Delta F_{140\ K}$) of ICA-17043-induced fluorescence change ($\Delta F_{ICA-17043}$) to 140 mM K^+-induced fluorescence change ($\Delta F_{140\ K}$). The numbers of used for the experiments are shown in parentheses. **: $P < 0.01$ versus Ox–/–.

Figure S3 Up-regulation of $K_{Ca}3.1$ expression in $CD4^+$ ALN T-lymphocytes of Ox+/– and Ox+/+ mice. A fluorescent dual colour dot-plot of FITC-CD4 versus PE-$K_{Ca}3.1$ in fixed and permeabilized ALN lymphocytes was analyzed by FCM. Flow cytometry plots showing the expression levels of $K_{Ca}3.1$ in the gated $CD4^+$ cell population from Ox–/–, Ox+/– and Ox+/+ (C) ALNs. D, E: Flow cytometry plots showing the non-specific signals of anti-$K_{Ca}3.1$ antibody by use of pre-incubated anti-$K_{Ca}3.1$ antibody with excess antigen peptides (D) and showing the non-specific signals of PE-conjugated anti-rabbit IgG antibody (E). In C-E, transparent cell images (right, upper panels) and images of PE fluorescence (right, lower panels) were shown.

Figure S4 The effects of ICA-17043 on the auricular thickness and ALN weight in Ox+/+, and on the expression of $K_{Ca}3.1a$ and $K_{Ca}3.1b$ as well as the REST transcripts in the ALNs of Ox+/+. A: A: Auricular thickness (mm) in the vehicle control and ICA-17043-administered groups. B: ALN weight (mg) in the vehicle control and ICA-17043-administered groups. The results are expressed as the means ± SEM. The numbers used for the experiments are shown in parentheses. **: $P < 0.01$ versus vehicle control. C: Quantitative, real-time PCR assay for $K_{Ca}3.1a$ (open columns), $K_{Ca}3.1b$ (closed columns) and REST (hatched columns) in the ALNs of the vehicle control (n = 5) and ICA-17043 (3 mg/kg, s.c.)-administered (n = 6) groups. The results are expressed as the means ± SEM. **: $P < 0.01$ versus vehicle control.

Figure S5 The effects of the administration of TRAM-34 (10 mg/kg, s.c.) on ALN weight in Ox+/– (A), TRAM-34-induced depolarization responses in ALN T-lymphocytes of Ox+/– (B) and the expression of the $K_{Ca}3.1$ and REST transcripts in the ALNs of Ox+/– (C). TRAM-34 was administered 3 days after Ox sensitization, and 7 days after that the

sensitization experiments were performed. In A and B, the results are expressed as the means ± SEM. The numbers used for the experiments are shown in parentheses. **: $P < 0.01$ versus vehicle control. In C, the results are expressed as the means ± SEM ($n = 5$ for each). **: $P < 0.01$ versus vehicle control.

Figure S6 Expression of the $K_V1.3$ transcripts in ALN $CD4^+$ T-lymphocytes of Ox–/–, Ox+/– and Ox+/+ and measurement of margatoxin (MgTx)-sensitive $K_V1.3$ currents in ALN $CD4^+$ T-lymphocytes of Ox–/– and Ox+/+. A: Quantitative, real-time PCR assay for $K_V1.3$. The results are expressed as the means ± SEM ($n = 6$ for each). *: $P < 0.05$ versus Ox–/–, ##: $P < 0.01$ versus Ox+/–. B: Summarized data for 10 nM MgTx-sensitive current density in +40 mV determined by a ramp pulse protocol. C: 10 nM MgTx-sensitive $K_V1.3$ current induced by a 500 ms step pulse from –80 mV to +40 mV in ALN $CD4^+$ T-lymphocytes of Ox+/+. D: Summarized data for number of $K_V1.3$ channels per cell. In 'B' and 'D', the results are expressed as the means ± SEM. The number used for experiments are shown in parentheses. *: $P < 0.05$ versus Ox–/–.